Design and Flight Performance of the Orion Pre-Launch Navigation System

Renato Zanetti[1], Greg Holt[2], Robert Gay[3], and Christopher D'Souza[4]
NASA Johnson Space Center, Houston, Texas 77058.

Jastesh Sud[5] and Harvey Mamich[6]
Lockheed Martin Space Systems Company, Denver, CO 80201

Robert Gillis[7]
Emergent Space Technologies, Denver, CO 80201

The design of the NASA Orion's prelaunch navigation system is introduced, both for the first flight test, Exploration Flight Test-1 (EFT-1), and for the first planned Orion mission, Exploration Mission 1. A detailed trade off of possible design decisions are discussed and the choices made by Orion are presented. The actual performance of the navigation system during EFT-1 is presented together with the navigation flight-software data provided by Orion to the ground controllers in telemetry.

I. Introduction

Arguably one of the greatest successes and glorious applications of the fundamental work of Rudy Kalman on stochastic estimation [1, 2] is the Apollo onboard navigation filter [3]. The Orion capsule is NASA's current flagship human exploration vehicle, is reminiscent of Apollo, and is being designed to take humans back to the Moon and beyond. The first uncrewed Exploration Mission

[1] GN&C Autonomous Flight Systems Engineer, Aeroscience and Flight Mechanics Division, EG6, 2101 NASA Parkway
[2] Orion Navigation Co-Lead, Flight Operations Directorate, CM55, 2101 NASA Parkway.
[3] Orion Vehicle Integration Office Project Lead Engineer, JSC Technical Integration Office, EA4, 2101 NASA Parkway.
[4] Navigation Technical Discipline Lead, Aeroscience and Flight Mechanics Division, EG6, 2101 NASA Parkway.
[5] Software Engineer Staff, M/S B3003, P.O. Box 179
[6] Orion Navigation Co-Lead, M/S B3003, P.O. Box 179
[7] GN&C Engineer, M/S B3003, P.O. Box 179

(EM-1) is scheduled for 2018, while its first flight test, EFT-1 (Exploration Flight Test-1), was successfully completed on December 5th, 2014.

Reference [4] describes the navigation design of Orion's EFT-1 mission and the flight performance for the post-lift phase. This paper introduces and presents the complete design of the Orion pre-launch navigation system; both the EFT-1 design and the changes made for EM-1 and beyond. This work also documents the performance of the pre-launch navigation system during EFT-1 by presenting Orion's telemetry data and discussing the overall navigation results. Reference [5] introduced the preliminary EFT-1 navigation design, while pre-mission simulation performance was shown in reference. [6]. The UDU factorization as introduced by Bierman is employed in the filter design [7], and measurements are included as scalars employing the Carlson [8] and Agee-Turner [9] Rank-One updates. The possibility of considering some of the filter's states (rather than estimating all of them [10]) is included in the design [11].

Prior to launch the extended Kalman filter is initialized with the estimated vehicle's attitude from gyro compassing (coarse align algorithm) and an inertial position derived from the current time and the coordinates of the pad. This pre-launch navigation phase is called fine align and the only measurement active in this mode during EFT-1 was integrated velocity, which is a pseudo-measurement consisting of a zero change of Earth-referenced position over a 1 second interval. The GPS receiver measurements are not available during fine align because the vehicle, including the GPS antennas, is covered by the launch abort fairing. The main purpose of fine align is to better estimate the attitude in preparation for launch.

The two main contributions of this work are a detailed analysis of ground align measurements types to feed the Kalman filter and the introduction of a pad position measurement with fully correlated survey errors between the measurement and the filter's initial condition. This work also presents the actual flight telemetry data of Orion EFT-1, hence validating with actual mission data the design choices.

The fundamental sensor used during Coarse and Fine align is the Inertial Measurement Unit (IMU), whose EKF model is presented in Section II. The Coarse Align design is presented in III, while the pre-launch EKF design used for Fine Align is presented in Section IV. The EFT-1 flight

performance is presented in Section V followed by concluding remarks.

II. Inertial Measurement Unit

The sections presents the IMU measurement model, which includes both gyros and accelerometers.

A. The Gyro Model

The gyro is modeled in terms of the bias, scale factor, and non-orthogonality. It is taken as the alignment reference navigation sensor, therefore no gyro misalignment states are included. The non-orthogonality errors of the IMU case frame are expressed as

$$\mathbf{\Gamma}_g = \begin{bmatrix} 0 & \gamma_3^g & \gamma_2^g \\ \gamma_3^g & 0 & \gamma_1^g \\ \gamma_2^g & \gamma_1^g & 0 \end{bmatrix}$$

The gyro scale factor represents the error in conversion from raw sensor outputs (gyro digitizer pulses) to engineering units. The scale-factor error is modeled as a first-order Markov process in terms of a diagonal matrix given as

$$\mathbf{S}_g = \begin{bmatrix} s_x^g & 0 & 0 \\ 0 & s_y^g & 0 \\ 0 & 0 & s_z^g \end{bmatrix}$$

Similarly, the gyro bias error is modeled as a first-order vector Markov processes as

$$\boldsymbol{b}_g = \begin{bmatrix} b_x^g \\ b_y^g \\ b_z^g \end{bmatrix}$$

The gyro angular random walk is represented by $\boldsymbol{\nu}_g$; the model of the gyro's angular velocity measurement $\tilde{\boldsymbol{\omega}}^c$ is given by

$$\tilde{\boldsymbol{\omega}}^c \;=\; (\mathbf{I}_3 + \mathbf{\Gamma}_g + \mathbf{S}_g)\,(\boldsymbol{\omega}^c + \boldsymbol{b}_g + \boldsymbol{\nu}_g) = (\mathbf{I}_3 + \mathbf{\Delta}_g)\,(\boldsymbol{\omega}^c + \boldsymbol{b}_g + \boldsymbol{\nu}_g) \tag{1}$$

where $\mathbf{I}_3$ is a 3×3 identity matrix, the superscript c indicates that this is a measurement expressed in case-frame co-ordinates, and $\boldsymbol{\omega}^c$ is the 'true' angular velocity in the case frame. Internally the

actual measurement from the gyros is an integrated angular rate that, which, if used directly by the Kalman filter, would produce a suboptimal estimator [12]. Therefore, a coning compensation algorithm [13] is used internally by the sensor's firmware.such as the effective measurement is given by

$$\Delta\tilde{\boldsymbol{\theta}}_k^c = \Delta\tilde{\boldsymbol{\theta}}_{c_{k-1}}^{c_k} = \int_{t_{k-1}}^{t_k} \tilde{\boldsymbol{\omega}}^c(\tau) + \frac{1}{2}\Delta\tilde{\boldsymbol{\theta}}_{c_{k-1}}^{c(\tau)} \times \tilde{\boldsymbol{\omega}}^c(\tau)\, d\tau \qquad \Delta\tilde{\boldsymbol{\theta}}_{c_{k-1}}^{c_{k-1}} = \mathbf{0} \tag{2}$$

B. The Accelerometer Model

Similar to the gyros, the accelerometer scale factor represents the error in conversion from raw sensor outputs (accelerometer digitizer pulses) to engineering units and are modeled as a first-order Markov process in terms of a diagonal matrix given as

$$\mathbf{S}_a = \begin{bmatrix} s_x^a & 0 & 0 \\ 0 & s_y^a & 0 \\ 0 & 0 & s_z^a \end{bmatrix}$$

As mentioned in the previous section, the gyro is taken as the aligned sensor while the accelerometer misalignment relative to the gyro is taken into account. The accelerometer misalignment and nonorthogonality errors are combined and expressed in terms of six different small angles as:

$$\boldsymbol{\Xi}_a = \begin{bmatrix} 0 & \xi_{xy}^a & \xi_{xz}^a \\ \xi_{yx}^a & 0 & \xi_{yz}^a \\ \xi_{zx}^a & \xi_{zy}^a & 0 \end{bmatrix}$$

The bias errors are modeled as a first-order Gauss-Markov processes as

$$\boldsymbol{b}_a = \begin{bmatrix} b_x^a \\ b_y^a \\ b_z^a \end{bmatrix}$$

The accelerometer measurements, $\tilde{\boldsymbol{a}}^c$ are modeled as:

$$\tilde{\boldsymbol{a}}^c = (\mathbf{I}_3 + \boldsymbol{S}_a + \boldsymbol{\Xi}_a)\,(\boldsymbol{a}^c + \boldsymbol{b}_a + \boldsymbol{\nu}_a) \tag{3}$$

where $\boldsymbol{a}^c$ is the 'true' non-gravitational acceleration in the case frame. The quantity $\boldsymbol{\nu}_a$ is the velocity random walk.

The actual measurement is accumulated acceleration in the case frame, $\Delta\tilde{\mathbf{v}}^c$, which is mapped to the end of its corresponding time interval by the sculling algorithm within the IMU firmware

$$\Delta\tilde{\mathbf{v}}_k^c = \Delta\tilde{\mathbf{v}}_{c_{k-1}}^{c_k} = \int_{t_{k-1}}^{t_k} \mathbf{T}_{c(t)}^{c_k} \tilde{\mathbf{a}}^c(t)\, dt \tag{4}$$

where $\Delta\tilde{\mathbf{v}}_k^c$ covers the time interval from t_{k-1} to t_k and $c(t)$ is the instantaneous case frame.

The transformation matrix $\mathbf{T}_{c(t)}^{c_k}$ takes vector coordinates from the case frame at time t to the case frame at time t_k.

III. Coarse Align Design

The Coarse Align Computer Software Unit (CSU) main purpose is to compute an initial estimate of the attitude of the Orion vehicle while on the pad to initialize the EKF. The output attitude is based on a simple filtering of high rate IMU data with the assumption that the vehicle has zero velocity in the Earth-fixed frame.

Orion IMU sensor internal sampling is done at a very high rate to accommodate high rate compensations such as coning, sculling, size effect, and accelerometer digitizer asymmetry compensation. The high rate data is used to form compensated 200 Hz delta angles and delta velocities in the body frame. The 200 Hz data is organized in buffers and passed to the Orion flight computer at 40 Hz. Low pass second order filters are applied to the IMU measurements to remove noise and oscillatory motion due to wind (twist and sway).

The expected output of the Coarse Alignment, $\mathbf{T}_e^c$, is the attitude of the IMU case frame with respect to the Earth-fixed frame (e, or International Terrestrial Reference Frame, ITRF). An intermediate calculation is T_{ned}^c, that represents the transformation matrix of the vehicle attitude with respect to the North-East-Down (NED) frame.

$$\mathbf{T}_e^c = \mathbf{T}_{ned}^c \times \mathbf{T}_e^{ned}$$

The transformation matrix $\mathbf{T}_e^{ned}$ is determined from the surveyed coordinates of the pad.

A potential algorithm singularity exists if $\Delta\mathbf{v}_{filt}^c$ and $\Delta\boldsymbol{\theta}_{filt}^c$ vectors are co-linear. This condition does not occur unless the alignment is done near the north or south pole, however the software

contains a check to ensure the $|\Delta\boldsymbol{\theta}^c_{filt} \times \hat{\mathbf{U}}^c|$ is of reasonable size prior to computing $\hat{\mathbf{E}}^c$.

IV. Fine Align Design

As previously mentioned, the goal of fine align is to improve the attitude estimate prior to launch. The only measurement available is the IMU measurement which is used by an EKF in conjunction with a pseudomeasurement relating the information that, prior to lift-off, the vehicle is not moving with respect to the pad.

The EKF software is shared between fine align operations and atmospheric flight operations (ascent, ascent aborts, and entry); all measurements are incorporated in the navigation solution at 1Hz, which is the GPS measurement rate used during atmospheric flight. The attitude control algorithm used during atmospheric flight (ascent aborts and entry) necessitates estimates from the navigation solution at a higher rate than 1 Hz, thus delta velocity delta attitude accumulator (DVDAAccum) Computer Software Unit (CSU) is used as the high-rate IMU accumulator and attitude propagator complement to EKF CSUs in the 1 Hz rate group. The vehicle attitude is propagated forward in time through the use of accumulated sensed $\Delta\boldsymbol{\theta}$ data. The CSU also accumulates $\Delta\mathbf{v}$ measurements which are used by the Position and Velocity Fast Propagator (PVPropFast) to compute high rate position and velocity for downstream users. The attitude of DVDAAccum and the state of PVPropFast are re-synched to the 1 Hz rate group estimate each second.

DVDAAccum receives feedback data from the 1 Hz EKF CSUs and uses it to perform an update. During the update phase DVDAAccum replaces the estimates of the IMU errors with the most current values from the EKF, transforms the values of the inertial accumulated delta velocity into the updated inertial frame, and updates the inertial to Orion body attitude with the information from the filter.

As mentioned above, the Orion fine alignment algorithm utilizes the same Extended Kalman Filter architecture and CSU as that used for atmospheric navigation (named ATMEKF). This paper presents the design of the fine align portion of the algorithm and trade studies that were conducted between three different type of fine align measurements: Integrated Velocity (IV), Zero Velocity (ZV), and Pad Position (Pos). All these measurements are pseudomeasurents (no sensor exists that

produces them) instead the measurements are derived from the known fact that the vehicle is not moving with respect to the launch pad. Hence the actual measurement utilized in the filter is the theoretical value corresponding to absence of motion and the measurement error is given by the variation from this theoretical value due to twist and sway oscillations of the launch stack. This motion is forced by wind and is a function of the bending modes of the launch system.

The navigation center of computations is given by the IMU location. During EFT-1, the Orion EKF used an IV measurement during the fine align phase. For EM1 and beyond, three possible solutions are considered:

1. The IV measurement returns the change in Earth Centered Earth Fixed (ECEF) position over a specified amount of time, typically the call rate of the EKF, which for EFT-1 is one second. The processed measurement is always given by the nominal value of zero. The measurement noise is given by the change of position of the IMU over one second due to twist and sway of the stack.

2. The pad position (Pos) measurement returns the planet-fixed position of the IMU. This is also a "fake" measurement always set to the nominal location. The measurement error is comprised not only to the twist and sway motion, but also of the survey error of the pad location. Therefore the measurement error has two distinct contributors, a varying component due to the stack oscillations (modeled as white) and a repeatable component due to the survey errors (modeled as a random bias).

3. The zero velocity (ZV) measurement returns the instantaneous planet-fixed velocity of the IMU. This is also always set to the nominal value of zero. The measurement noise is given by the true velocity of the IMU due to twist and sway of the stack.

In all three cases the twist and sway motion is treated as white noise rather than colored noise in order to keep the state space smaller and save computations. Thousands of simulated worst-case scenario robustness analysis runs were performed sweeping large ranges of twist and sway frequencies and amplitudes. These runs showed the filter robustness with respect to these inputs.

A. Integrated Velocity

Given the current inertial position $\mathbf{r}^i$ at time t, the prior inertial position $\mathbf{r}_0^i$, as well as the transformation matrix between Earth-fixed and inertial ($\mathbf{T}_i^e$), the IV measurement is given by

$$\mathbf{y}_{IV} = \mathbf{h}_{IV}(\mathbf{x}, \mathbf{x}_0, t) + \boldsymbol{\eta}_{IV} = \mathbf{T}_i^e(t)\,\mathbf{r}^i - \mathbf{T}_i^e(t_0)\,\mathbf{r}_0^i + \boldsymbol{\eta}_{IV} = \mathbf{0} \tag{5}$$

where $\mathbf{h}_{IV}(\mathbf{x}, \mathbf{x}_0, t)$ is the measurement model and $\boldsymbol{\eta}_{IV}$ is the measurement noise which exactly cancels out the motion due to twist and sway. The estimated measurement is given by

$$\hat{\mathbf{y}}_{IV} = \mathbf{h}_{IV}(\hat{\mathbf{x}}, \hat{\mathbf{x}}_0, t) = \mathbf{T}_i^e(t)\,\hat{\mathbf{r}}^i - \mathbf{T}_i^e(t_0)\,\hat{\mathbf{r}}_0^i \tag{6}$$

Notice that this measurement is nonlinear, potentially highly-nonlinear, since in order to calculate $\hat{\mathbf{r}}_0^i$ it is necessary to back-integrate the nonlinear equations of motion that also contain the estimates of the IMU error parameters. The measurement residual is

$$\boldsymbol{\epsilon}_{IV} = \mathbf{y}_{IV} - \hat{\mathbf{y}}_{IV} \tag{7}$$

As a first order approximation (used to obtain the IV measurement partials or measurement mapping matrix $\mathbf{H}_{IV}$)

$$\boldsymbol{\epsilon}_{IV} = \frac{\partial \mathbf{h}_{IV}}{\partial \mathbf{x}}(\mathbf{x} - \hat{\mathbf{x}}) + \frac{\partial \mathbf{h}_{IV}}{\partial \mathbf{x}_0}(\mathbf{x}_0 - \hat{\mathbf{x}}_0) + \boldsymbol{\eta}_{IV} \tag{8}$$

$$= \frac{\partial \mathbf{h}_{IV}}{\partial \mathbf{x}}\hat{\mathbf{x}} + \frac{\partial \mathbf{h}_{IV}}{\partial \mathbf{x}_0}\boldsymbol{\Phi}(t, t_0)\hat{\mathbf{x}} + \boldsymbol{\eta}_{IV} \tag{9}$$

$$= \mathbf{H}_{IV}(\hat{\mathbf{x}})\,(\mathbf{x} - \hat{\mathbf{x}}) + \boldsymbol{\eta}_{IV} \tag{10}$$

where $\mathbf{\Phi}(t, t_0)$ is the state transition matrix. With this in mind, the partial derivative of the IV measurement is as follows

$$\frac{\partial \mathbf{h}_{IV}}{\partial \mathbf{r}}(\hat{\mathbf{x}}) = \mathbf{T}_i^e(t) \; - \mathbf{T}_i^e(t_0)\, \Phi_{\mathbf{rr}}(t, t_0) \tag{11}$$

$$\frac{\partial \mathbf{h}_{IV}}{\partial \mathbf{v}}(\hat{\mathbf{x}}) = -\mathbf{T}_i^e(t_0)\, \Phi_{\mathbf{rv}}(t, t_0) \tag{12}$$

$$\frac{\partial \mathbf{h}_{IV}}{\partial \boldsymbol{\phi}}(\hat{\mathbf{x}}) = -\mathbf{T}_i^e(t_0)\, \Phi_{\mathbf{r}\boldsymbol{\phi}}(t, t_0) \tag{13}$$

$$\frac{\partial \mathbf{h}_{IV}}{\partial \mathbf{b}_a}(\hat{\mathbf{x}}) = -\mathbf{T}_i^e(t_0)\, \Phi_{\mathbf{rb}_a}(t, t_0) \tag{14}$$

$$\frac{\partial \mathbf{h}_{IV}}{\partial \mathbf{s}_a}(\hat{\mathbf{x}}) = -\mathbf{T}_i^e(t_0)\, \Phi_{\mathbf{rs}_a}(t, t_0) \tag{15}$$

$$\frac{\partial \mathbf{h}_{IV}}{\partial \boldsymbol{\xi}_a}(\hat{\mathbf{x}}) = -\mathbf{T}_i^e(t_0)\, \Phi_{\mathbf{r}\boldsymbol{\xi}_a}(t, t_0) \tag{16}$$

$$\frac{\partial \mathbf{h}_{IV}}{\partial \mathbf{b}_g}(\hat{\mathbf{x}}) = -\mathbf{T}_i^e(t_0)\, \Phi_{\mathbf{rb}_g}(t, t_0) \tag{17}$$

$$\frac{\partial \mathbf{h}_{IV}}{\partial \mathbf{s}_g}(\hat{\mathbf{x}}) = -\mathbf{T}_i^e(t_0)\, \Phi_{\mathbf{rs}_g}(t, t_0) \tag{18}$$

$$\frac{\partial \mathbf{h}_{IV}}{\partial \boldsymbol{\gamma}_g}(\hat{\mathbf{x}}) = -\mathbf{T}_i^e(t_0)\, \Phi_{\mathbf{r}\boldsymbol{\gamma}_g}(t, t_0) \tag{19}$$

Because of the back-propagation, this measurement is nonlinear in nature. Due to the oscillatory motion in the flex modes of the stack this nonlinearity could be potentially severe, although severe nonlinearities are not expected over one second intervals (nor were they experienced during EFT-1).

B. Pad Position Measurement

The position measurement is expressed as follows:

$$\mathbf{y}_{Pos} = \mathbf{h}_{Pos}(\mathbf{x}, t) + \boldsymbol{\eta}_{Pos} = \mathbf{T}_i^e(t)\, \mathbf{r}^i + \mathbf{b}_{pad} + \boldsymbol{\eta}_{Pos} \tag{20}$$

where $\mathbf{b}_{pad}$ is the launch pad location survey error and $\boldsymbol{\eta}_{Pos}$ is the measurement noise which exactly cancels out the motion due to twist and sway. The estimated measurement is given by

$$\hat{\mathbf{y}}_{Pos} = \mathbf{h}_{Pos}(\hat{\mathbf{x}}, t) = \mathbf{T}_i^e(t)\, \hat{\mathbf{r}}^i + \hat{\mathbf{b}}_{pad} \tag{21}$$

The measurement residual is

$$\boldsymbol{\epsilon}_{Pos} = \mathbf{y}_{Pos} - \hat{\mathbf{y}}_{Pos} = \mathbf{H}_{Pos}(\hat{\mathbf{x}})\, \hat{\mathbf{x}} + \boldsymbol{\eta}_{Pos} \tag{22}$$

With this in mind, the partial derivative of the position measurement is as follows

$$\frac{\partial \mathbf{h}_{Pos}}{\partial \mathbf{r}}(\hat{\mathbf{x}}) = \mathbf{T}_i^e(t) \tag{23}$$

$$\frac{\partial \mathbf{h}_{Pos}}{\partial \mathbf{b}_{pad}}(\hat{\mathbf{x}}) = \mathbf{I}_{3\times 3} \tag{24}$$

Notice that this is a linear measurement and the measurement noise is given by the displacement due to sway.

C. Zero Velocity

The zero velocity measurement is expressed as follows:

$$\mathbf{y}_{ZV} = \mathbf{h}_{ZV}(\mathbf{x}, t) + \boldsymbol{\eta}_{ZV} = \mathbf{T}_i^e(t)\ \left(\mathbf{v}^i - \boldsymbol{\omega}_E^i \times \mathbf{r}^i\right) + \boldsymbol{\eta}_{ZV} = \mathbf{0} \tag{25}$$

where $\boldsymbol{\omega}_E^i$ is the Earth angular velocity vector and $\boldsymbol{\eta}_{ZV}$ is the measurement noise which exactly cancels out the motion due to twist and sway. The estimated measurement is given by

$$\hat{\mathbf{y}}_{ZV} = \mathbf{h}_{ZV}(\hat{\mathbf{x}}, t) = \mathbf{T}_i^e(t)\ \left(\hat{\mathbf{v}}^i - \boldsymbol{\omega}_E^i \times \hat{\mathbf{r}}^i\right) \tag{26}$$

The measurement residual is

$$\boldsymbol{\epsilon}_{ZV} = \mathbf{y}_{ZV} - \hat{\mathbf{y}}_{ZV} = \mathbf{H}_{ZV}(\hat{\mathbf{x}})\,\hat{\mathbf{x}} + \boldsymbol{\eta}_{ZV} \tag{27}$$

With this in mind, the partial derivative of the zero velocity measurement is as follows

$$\frac{\partial \mathbf{h}_{ZV}}{\partial \mathbf{r}}(\hat{\mathbf{x}}) = \mathbf{T}_i^e(t)\,[\boldsymbol{\omega}_E^i\times] \tag{28}$$

$$\frac{\partial \mathbf{h}_{ZV}}{\partial \mathbf{v}}(\hat{\mathbf{x}}) = \mathbf{T}_i^e(t) \tag{29}$$

Notice that this is a linear measurement and the measurement noise is given by the velocity of the oscillation due to sway.

D. Fine Align Measurement Trade

During factor-of-safety performed prior to EFT-1, the results showed that the IV measurement is subject to divergence under some higher-than-expected frequency cases. These cases were deemed extremely unlikely; furthermore the performance of fine align is monitored from the ground which has the ability to scrub the launch if the atmospheric conditions create excessive oscillatory motion

of the stack. While robustness to the amplitude of the oscillations can be achieved via tuning of the value of the IV measurement noise variance, increasing robustness to very large frequency variations in the oscillations has no obvious solution. The problem arises from the fact that high frequency of oscillation make the IV measurement nonlinearities more pronounced.

The IV measurement is inherently a measurement of velocity, or at least average velocity, since it measures the change in position. Therefore this measurement type provides very little information on the position of the vehicle. This fact can be seen by the gradual increase of the position estimation error covariance produced by the filter during fine align. Figure 1 shows linear covariance analysis results, including the increase in position uncertainty (Fig. 6 in the next section contains the telemetry covariance from the day of flight and shows a very close match with the linear covariance analysis results). Very long pad operations can cause the position estimation error to become excessively large, forcing the ground to send a position re-anchoring command prior to launch, as routinely done in Space Shuttle missions. Two options are possible for the re-anchoring: overwriting the state only, hence having a good state estimate but a large, over-conservative estimation error covariance, or re-initializing the position error covariance as well, hence losing the correlations between position and all other states.

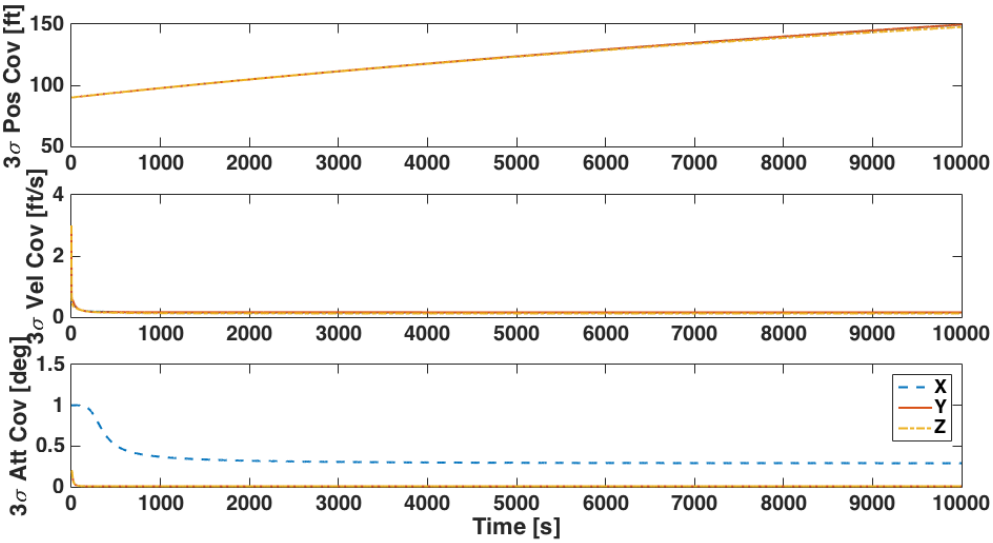

Fig. 1 Linear covariance analysis showing position, velocity, and attitude 3σ Covariance while processing IV measurements

During very long pad alignment times, the position covariance eventually ceases to increase and asymptotically settles to a large value. The reason is that some position observability is extracted from the gravity model and the measurement of gravity by the accelerometer as well as from the direction of Earth's rotation measured by the gyros. As shown in Fig. 2, it takes a very long time for the error to reach steady state. Since the position of the pad is known within a certain tolerance, it is preferable that the position estimate of the filter and its uncertainty are constant at the pad survey error value rather than having a decreasing accuracy.

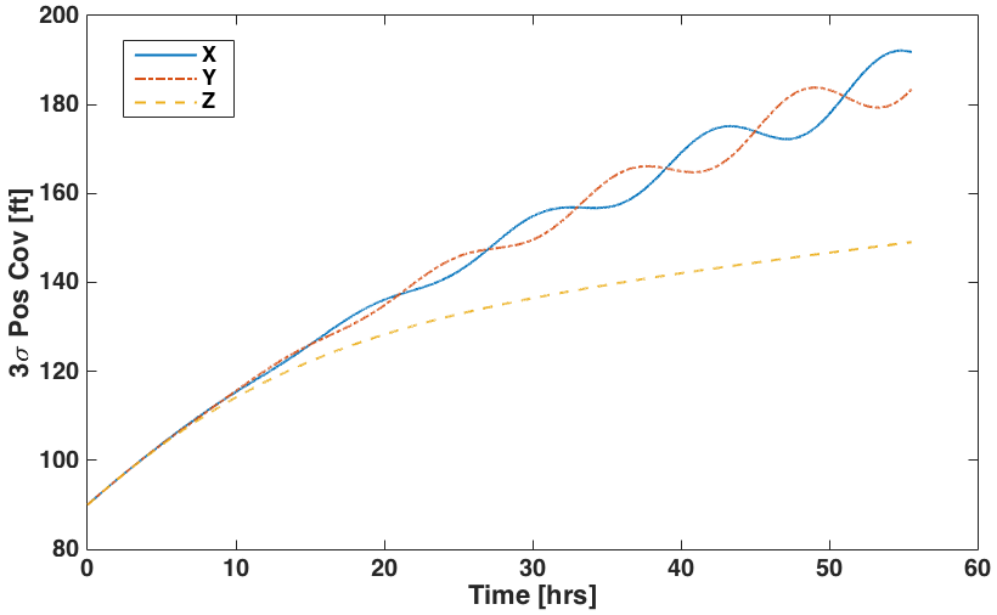

Fig. 2 Linear covariance analysis showing position 3σ Covariance for a very long fine align duration

The most important aspect of the fine align measurement trade is whether or not a position re-anchoring is necessary. Ground commands not only increase the complexity of the code, but, more importantly, require controllers to spend considerable time developing and studying flight rules to handle various scenarios. A position re-anchoring can be automatically forced immediately prior to launch, however this has the unwanted side effect of either a largely conservative position covariance, or cancelling all the correlation between position and other states. These correlations are used to estimate the other states from GPS pseudorange measurements during ascent. The pad position measurement keeps the estimated position error covariance constant during ground

align operations, and never necessitates re-anchoring. Figure 3 shows the linear covariance analysis performance assessment of the navigation filter using pad position measurements, where it can be seen that the position uncertainty stays constant. The 3σ steady-state velocity uncertainty is 0.12 ft/s for the IV measurement shown in Fig. 1 and 0.04 ft/s for Pos in Fig. 3; both use a measurement noise 1σ value of 0.4 ft. The measurement error for the pad position measurement is limited by half the oscillation due to twist and sway (the measurement error is the difference between the position with oscillations and the position without). The measurement noise for the IV measurement is the difference between the positions at two consecutive times, hence it can be as big as a full oscillation. Feeding the two measurement types with the same value of measurement noise results in a conservative analysis for the Pad position measurement, which is still able to estimate velocity three times better than IV. However, since velocity estimation accuracy is already within the launch requirement, this benefit of the Pos measurement is weighted low in the trade. Both IV and ZV measurement have very similar performance and weak position observability, which comes from either the fact that gravity is a function of position or from $\omega \times \mathbf{r}$ due to Earth's rotation; both have a very low sensitivity to position changes.

In all aspects of flight-software design, it is very important to keep the algorithm as simple as possible while meeting requirements. ZV and Pos measurements are both linear, do not require back propagation of the state, and hence are significantly simpler to implement than IV. Of the two, ZV is the simpler because it does not require the addition of a bias error state. The pad location estimate is affected by survey error, therefore processing the measurement every second results in a repeatable measurement error (i.e. non-white); furthermore this survey value is used to initialize the filter, hence the initial error is correlated to the measurement error. The need for extra states, and hence a larger covariance matrix and more computations, is mitigated by the fact that GPS measurement are not processed while on the pad; GPS measurement processing necessitate the inclusion of clock bias and drift states (single differencing techniques exist to eliminate the need of clock states in the EKF but they are not used in Orion). Three of the four GPS clock bias and drift states (one pari for each of the two receivers) are recycled as pad position bias states. As a result the pad position measurement does not require any increase on the size of the ATMEKF state

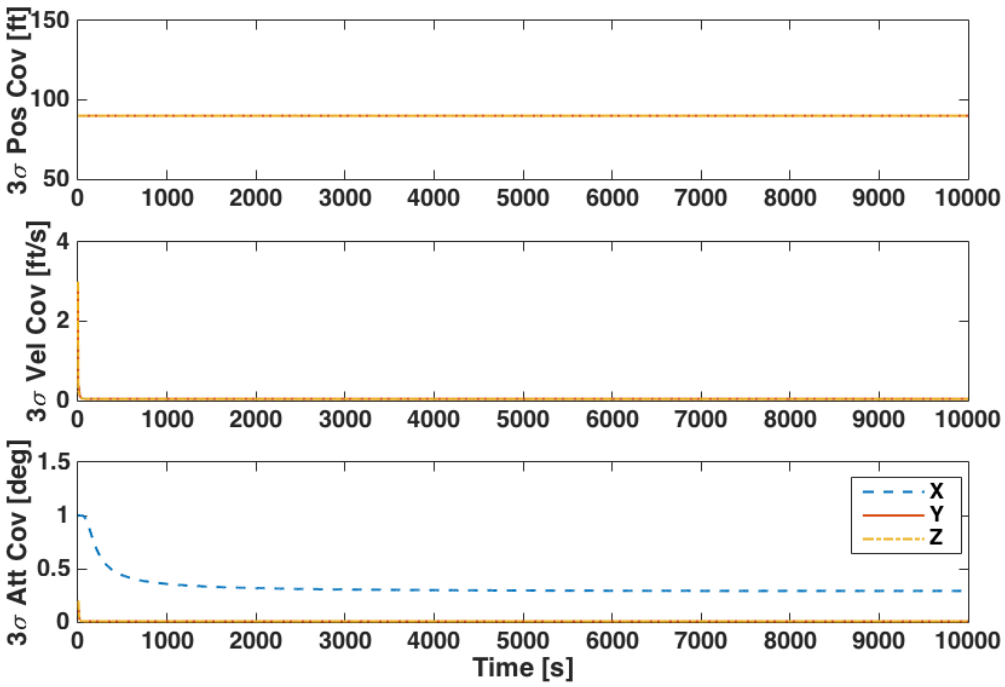

Fig. 3 Linear covariance analysis showing position, velocity, and attitude 3σ Covariance while processing Pad Position measurements

vector and covariance.

While filter divergence is a very serious issue that must be taken into consideration, the situations in which IV measurement caused divergence of the filter are extreme and deemed very unlikely to occur. Even if these conditions occur, the ground would be able to postpone the launch. Therefore divergence issues are the lowest weighted element of this trade. Pad position and ZV are linear measurements, therefore, if properly tuned, they cannot cause divergence during a measurement update (divergence during the measurement update is due to improper tuning or large nonlinear effects).

Given these four aspects of the trade, pad position measurements were deemed the best solution for Orion going forward and replace IV for Exploration Mission 1 and beyond. Table 1 shows the matrix of the trade.

Trade Factor	Trade Weight	IV	Pos	ZV
Avoid position re-anchor	High	NO	**YES**	NO
Lower algorithm complexity	Medium	NO	NO	**YES**
Higher Velocity Estimation Accuracy	Low	NO	**YES**	NO
Avoid potential divergence	Low	NO	**YES**	NO

Table 1 Fine Align Measurements Trade Matrix

E. Exploration Mission I Design

The Orion atmospheric extended Kalman filter (ATMEKF) processes all available observations each cycle to estimate position, velocity, and alignment, along with the measurement error parameters. All inertial sensor error estimates are fed back as corrections each cycle during the INS state correction process. The UDU algorithm is used in the ATMEKF processing to avoid any possible numerical instability in the covariance matrix.

From the trade study discussed above, the pad position measurement is processed by the filter. The observation is based on the fact that, during ground alignment, the navigation base is not moving with respect to Earth, other than twist and sway. The surveyed position of the stack is therefore used as an external measurement and it is compared to the propagated position using gravity and IMU data. Two errors affect the measurement. The first is due to oscillations because of twist and sway, this error source is aleatory in nature and modeled as white noise. The second source of error is repeatable, and is given by the survey error of the pad location together with the error in establishing the position of the IMUs with respect to the pad. This error is accounted for as a state in the filter.

The normalized squared measurement residuals values for each of the three components of the position observation are calculated prior to processing any observations, normalization is with respect to the filter's predicted residual standard deviation. If any of the three values exceeds the limit, all observation components are discarded for this cycle.

The state vector components are divided in dynamic-states, $\mathcal{X}$, and parameter-states (IMU errors and GPS PR errors), $\mathcal{B}$. Parameter-states differ from the other states in that they are

modeled as first order Markov processes, therefore their time evolution is known analytically and does not necessitate numerical integration. In addition, their state transition matrix is also known analytically and it is very sparse, making their covariance matrix propagation extremely numerically efficient.

$$\mathbf{X} = \begin{bmatrix} \mathcal{X}^T & \mathcal{B}^T \end{bmatrix}^T \tag{30}$$

The attitude is included as a state in the filter in order to properly model the coupling inherent in a strap-down IMU. As stated earlier the parameter-states are modeled as first-order Gauss-Markov processes and use a much more efficient computational algorithm for the update of the covariance matrix. Tables 2 and 3 list the states and parameters within the Atmospheric EKF. Through sensitivity analysis, it was determined that accelerometer misalignment and non-orthogonality states are not a significant contributor to the overall uncertainty and therefore are not included in the filter state space.

State	Number of elements	Description
Position	3	Position vector in inertial coordinates
Velocity	3	Velocity vector in inertial coordinate
Attitude	3	Multiplicative attitude deviation state
Clock Bias and Drift	4	One pair per receiver, three of these states are used as pad position bias states during fine align

Table 2 Atmospheric Navigation States

Position, velocity, and attitude states and their covariance are initialized as appropriate directly from data provided to the CSU. During Pad initialization scenarios, states 10 to 12 are initialized as pad bias states. The pad position measurement is expressed in Earth-fixed coordinates and is modeled as

$$\mathbf{y}_{pad} = \mathbf{r}^e + \mathbf{b}^e_{pad} + \boldsymbol{\eta}_{pad}$$

where $\mathbf{r}^e$ is the ECEF position vector, $\mathbf{b}^e_{pad}$ is the survey error of the pad position, and $\boldsymbol{\eta}_{pad}$ is the non-repeatable error of the measurement. The filter is initialized with the pad surveyed position

Parameter	Number of elements
gyro bias	3
gyro scale factor	3
gyro non-orthogonality	3
accel bias	3
accel scale factor	3
pseudorange bias	12

Table 3 Atmospheric Navigation Parameters

coordinated in the inertial frame, that is, the initial position estimate is given by

$$\hat{\mathbf{r}}(t_0) = \mathbf{T}_e^i(t_0)\,\mathbf{y}_{pad}$$

where $\mathbf{T}_e^i$ is the DCM transforming inertial coordinates into Earth-fixed coordinates, therefore the initial position estimation error $\mathbf{e}_r(t_0)$ is given by

$$\mathbf{e}_r(t_0) = \mathbf{r}(t_0) - \hat{\mathbf{r}}(t_0) = \mathbf{T}_e^i(t_0)\mathbf{r}^e - \mathbf{T}_e^i(t_0)(\mathbf{r}^e + \mathbf{b}_{pad}^e + \boldsymbol{\eta}_{pad}) \tag{31}$$

$$= -\mathbf{T}_e^i(t_0)\mathbf{b}_{pad}^e - \mathbf{T}_e^i(t_0)\boldsymbol{\eta}_{pad} = -\mathbf{T}_e^i(t_0)\mathbf{e}_{b_{pad}}^e - \mathbf{T}_e^i(t_0)\boldsymbol{\eta}_{pad} \tag{32}$$

The last equality holds because the initial estimated pad survey error is zero (otherwise the estimate error would be subtracted from the estimated position resulting in a new estimated position with zero estimated error). Equation (32) shows the correlation between the initial position and the survey error state, from it we deduce the values for the following elements of the initial covariance matrix

$$\mathbf{P}_0(b_{pad}, b_{pad}) = \mathbf{T}_i^e(t_0)\;\mathbf{P}_0(r,r)\;\mathbf{T}_e^i(t_0) \tag{33}$$

$$\mathbf{P}_0(X, b_{pad}) = \mathbf{P}_0(X,r)\;\mathbf{T}_e^i(t_0) \tag{34}$$

$$\mathbf{P}_0(b_{pad}, X) = \mathbf{T}_i^e(t_0)\;\mathbf{P}_0(r,X) \tag{35}$$

where $\mathbf{P}_0(b_{pad}, b_{pad})$ is the 3×3 covariance of the pad survey error state, $\mathbf{P}_0(r,r)$ is the 3×3 initial covariance of the position state, $\mathbf{P}_0(X, b_{pad})$ is the cross covariance between any state X and the pad survey error state. Notice that the contribution of the covariance of $\boldsymbol{\eta}_{pad}$ is neglected during

initialization because is much smaller than the survey error. The resulting 12x12 position, velocity, attitude, and pad survey error covariance matrix is generally non-diagonal and is converted to its UDU factorization for the filter to use. Notice that this covariance is singular, however no issues arise from this fact. If desired, the covariance can be made non-singular by slightly increasing the position uncertainty by the covariance of $\boldsymbol{\eta}_{pad}$.

V. Pre-Launch EFT-1 Design and Performance

To reduce the computation burden, EFT-1 EKF design did not include GPS PR bias states, refer to Ref. [4] for more details on the post-liftoff portion of EFT-1 navigation design and performance. The state-space of EFT-1 navigation filter design is shown in Tables 4 and 5.

State	Number of elements	Description
Position	3	Position vector in inertial coordinates
Velocity	3	Velocity vector in inertial coordinate
Attitude	3	Multiplicative attitude deviation state
Clock Bias and Drift	2	Only one GPS receiver used in EFT-1

Table 4 EFT-1 EKF Navigation States

Parameter	Number of elements
gyro bias	3
gyro scale factor	3
gyro non-orthogonality	3
accel high-g bias	3
accel low-g bias	3
accel scale factor	3
accel misalignment and non-orthogonality	6

Table 5 EFT-1 EKF Navigation Parameters

The tuning of the fine align navigation phase for EFT-1 is nearly identical to that of the ascent

phase described in Ref. [4], in particular an 8×8 gravity field is used, and the process noise is given by the IMU Angular Random Walk and Velocity Random Walk values. As stated previously, the IMU states are modeled as first-order Gauss-Markov, a time constant of 4 hours was used (the total flight duration was 4.5 hours and these errors were expected to remain nearly constant). The IMU states process noise values are chosen in order to match the steady-state value of the Markov processes to the vendor's specification. The integrated velocity error is unique to fine align; it was determined that an eight inch displacement was the maximum oscillation of the IMU due to twist and sway motion on the pad, making the peak-to-peak error 16 inches. A one-sigma IV error of 0.4 ft was chosen for EFT-1, which places the worst possible displacement case at a four-sigma value.

Figure 4 shows the performance of the filter processing this measurement by means of the measurement residual (actual measurement minus estimated measurement) and their predicted 3σ standard deviation (dashed lines). It can be seen that the residuals are well within their predicted standard deviations, all of the measurements are accepted and zero rejections occur. The residuals are extremely small with respect to their predicted standard deviation, this suggests the filter is overly conservative. This fact was expected and a design choice shown through simulation to add robustness to large twist and sway motion of the launch vehicle. During the day of flight little to no twist and sway was observed. Figure 4 shows the results from Channel 1. A zoomed-in plot of the residuals from Channel 2 is shown in Figure 5. Throughout the flight the performance of the two channels is nearly identical, therefore only results from Channel 1 are shown for the remainder of this section.

Figure 6 shows the filter's position, velocity, and attitude covariance. Figures 7 and 8 show the accelerometer and gyro error states covariance, respectively. Figures 9 and 10 show the filter's estimates of the accelerometer and gyro errors, respectively. The performance is as expected.

Finally, Figures 11 to 13 show the position, velocity, and attitude estimates from the user parameters processor (UPP) which for the entire flight provided the outputs from channel 1. Notice that some IMU parameters are not observable by they are kept in the filter for two reasons. First they correctly condition the covariance. Second they become observable with GPS after the high dynamics of ascent builds correlations. Many plots of unobservable variances do not show all lines

because they are superimposed with each other.

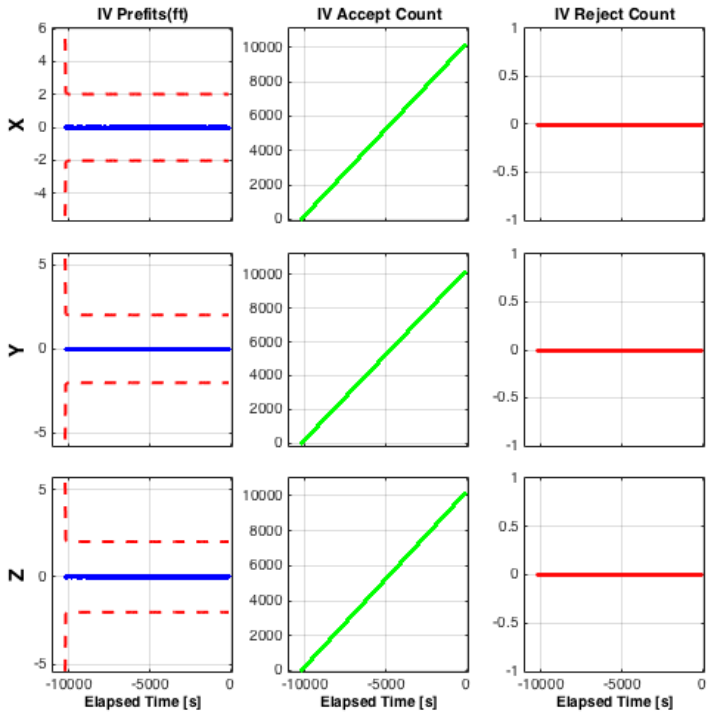

Fig. 4 FCM1-CH1 IV Measurements

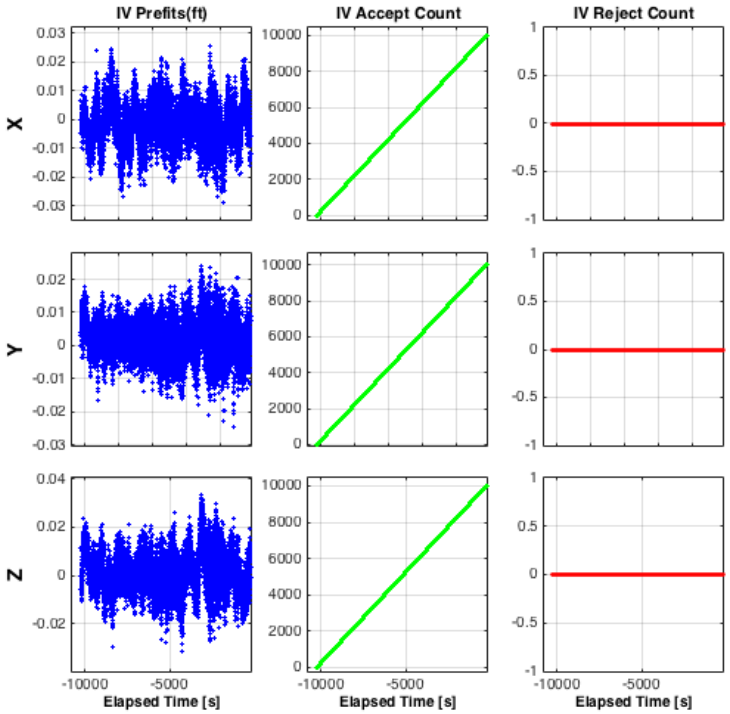

Fig. 5 FCM1-CH2 IV Measurements

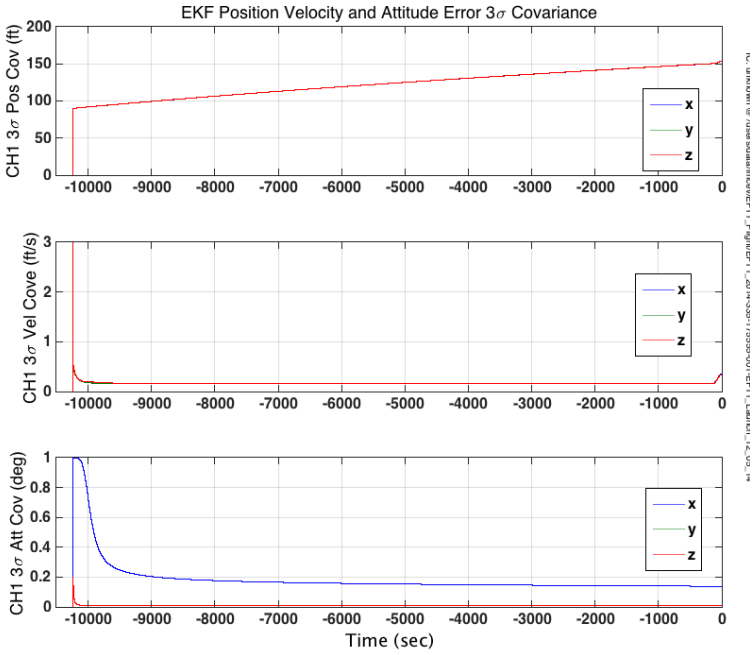

Fig. 6 FCM1-CH1 Position, Velocity, and Attitude 3σ Covariance

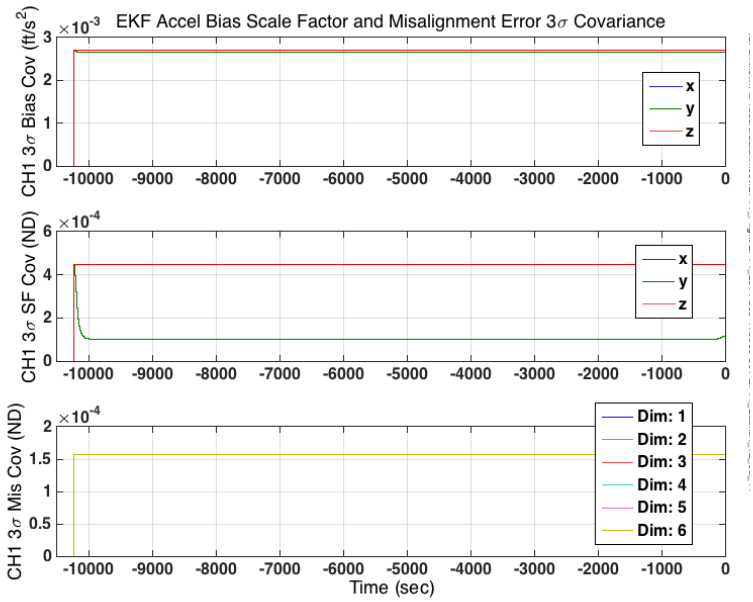

Fig. 7 FCM1-CH1 Accelerometer Bias, Scale Factor, and Misalignment 3σ Covariance

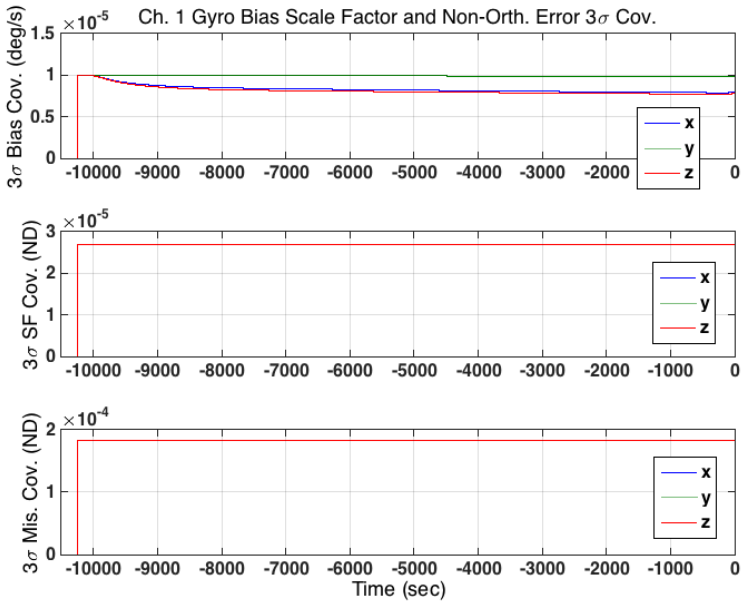

Fig. 8 FCM1-CH1 Gyro Bias, Scale Factor, and Non-Orthogonality 3σ Covariance

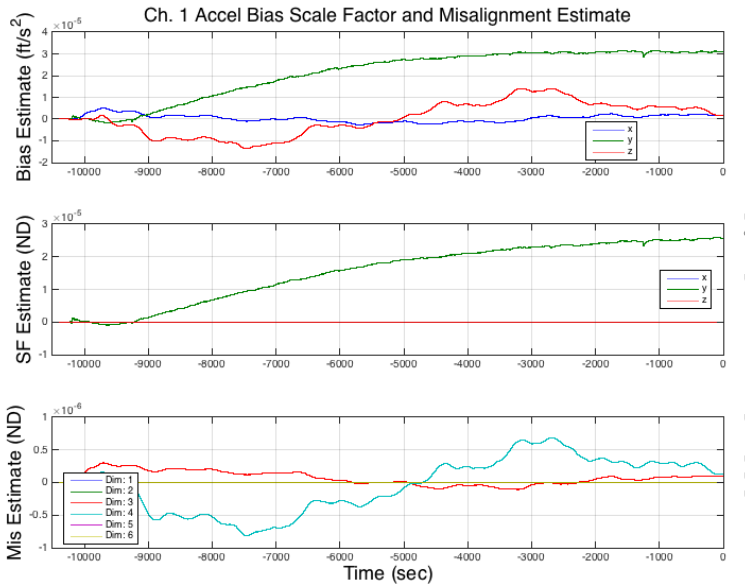

Fig. 9 FCM1-CH1 Accelerometer Bias, Scale Factor, and Misalignment Estimate

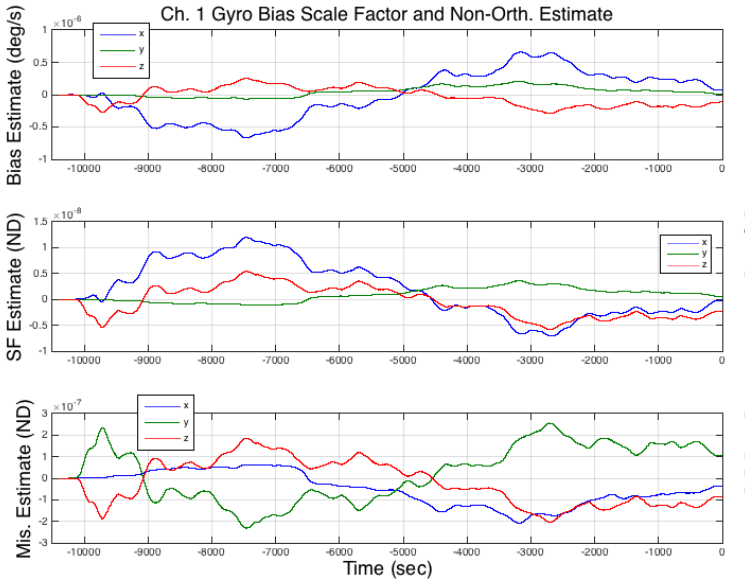

Fig. 10 FCM1-CH1 Gyro Bias, Scale Factor, and Non-Orthogonality Estimate

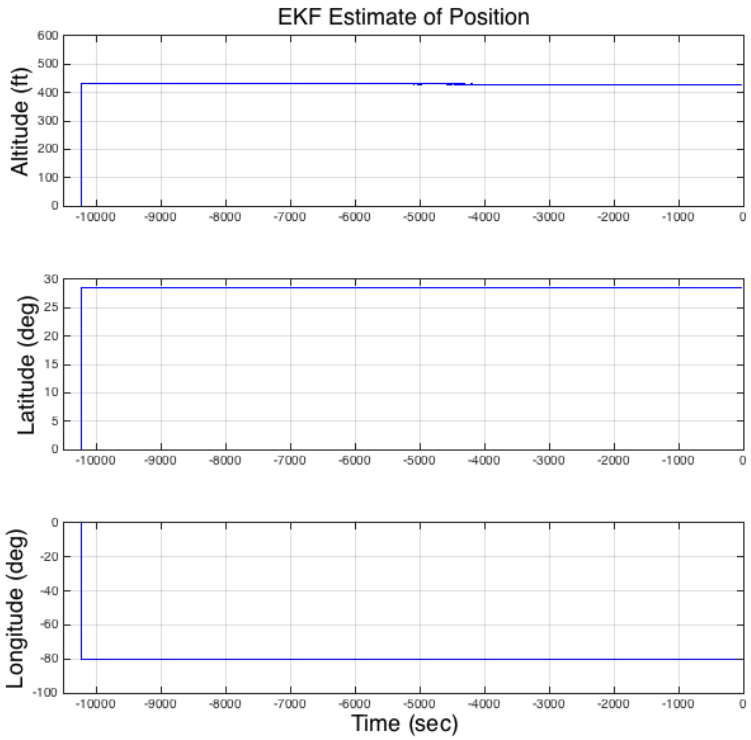

Fig. 11 FCM1-CH1 Position Estimate

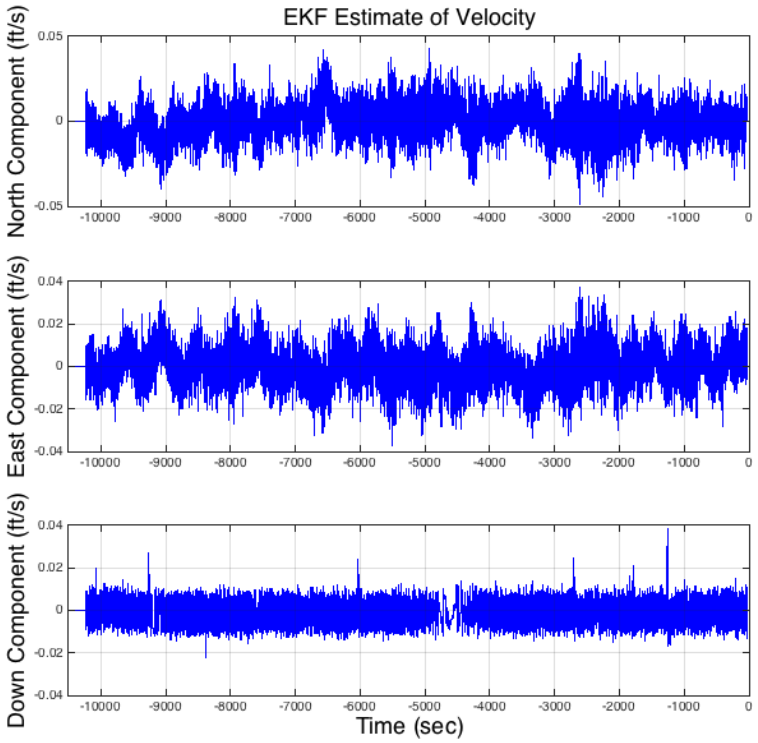

Fig. 12 FCM1-CH1 Velocity Estimate

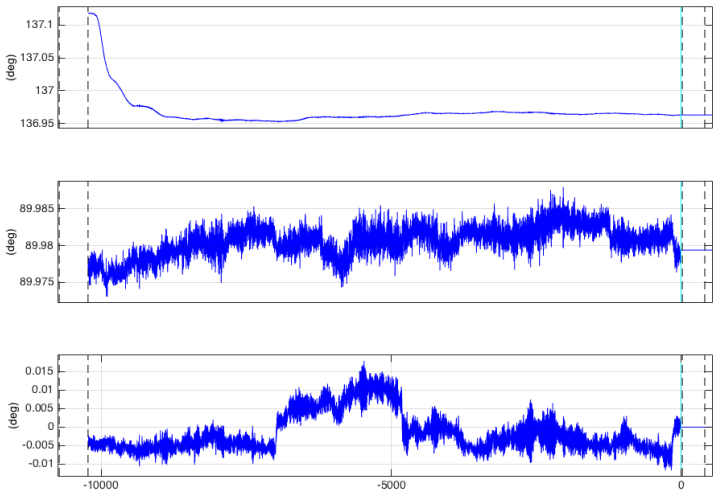

Fig. 13 FCM1-CH1 Attitude Estimate

VI. Conclusions

This paper documents the design of the Orion ground navigation system and presents its performance during Exploration Flight Test 1 (EFT-1). Characteristics of the EFT-1 design are introduced, and data from the flight is shown to validate the design choices. This data illustrates a flight in which the absolute navigation system performed as expected and produced a good state to guidance and control. No Integrated Velocity measurement rejections occurred in the filter and the measurement residuals were very low with respect to their predicted standard deviations. This fact is due to a combination of conservative tuning of this measurement and perfect weather during the day of launch. Design trades are also presented to justify the transition from the EFT-1 IV measurement to the use of Pad Position measurement during future Exploration Mission flights. The design of the EM1 ground alignment phase is presented in detail.

Aknowledgements

The authors are very thankful to Mike Begley, Daniel Kubitschek, Tim Straube, and Ellis King for their fundamental role in creating a successful Orion EFT1 pre-launch navigation system.

References

[1] Kalman, R. E., "A New Approach to Linear Filtering and Prediction Problems," *Journal of Basic Engineering*, Vol. 82, No. Series D, March 1960, pp. 35–45, doi:10.1115/1.3662552.

[2] Kalman, R. E. and Bucy, R. S., "New Results in Linear Filtering and Prediction," *Journal of Basic Engineering*, Vol. 83, No. Series D, March 1961, pp. 95–108, doi:10.1115/1.3658902.

[3] Battin, R. H., *An Introduction to the Mathematics and Methods of Astrodynamics*, AIAA Education Series, American Institude of Aeronautics and Astronautics, New York, NY, 1987. Pages 751–783.

[4] Zanetti, R., Holt, G. N., Gay, R. S., D'Souza, C., Sud, J., Mamich, H., Bagley, M., King, E., and Clark, F., "Orion Exploration Flight Test 1 (EFT1) Absolute Navigation Performance," *Journal of Guidance, Control, and Dynamics*, Accepted for publication 2016, doi: 10.2514/1.G002371.

[5] Sud, J., Gay, R., Holt, G., and Zanetti, R., "Orion Exploration Flight Test 1 (EFT1) Absolute Navigation Design," *Proceedings of the AAS Guidance and Control Conference*, Vol. 151 of *Advances in the Astronautical Sciences*, Breckenridge, CO, January 31–February 5, 2014 2014, pp. 499–509, AAS 14-092.

[6] Holt, G., Zanetti, R., and D'Souza, C., "Tuning and Robustness Analysis for the Orion Absolute Navigation System," Presented at the 2013 Guidance, Navigation, and Control Conference, Boston, Massachusetts, August 19–22 2013, AIAA-2013-4876, doi: 10.2514/6.2013-4876.

[7] Bierman, G. J., *Factorization Methods for Discrete Sequential Estimation*, Vol. 128 of *Mathematics in Sciences and Engineering*, Academic Press, 1978. Chapter 5.

[8] Carlson, N. A., "Fast Triangular Factorization of the Square Root Filter," *AIAA Journal*, Vol. 11, No. 9, September 1973, pp. 1259–1265, doi: 10.2514/3.6907.

[9] Agee, W. and Turner, R., "Triangular Decomposition of a Positive Definite Matrix Plus a Symmetric Dyad with Application to Kalman Filtering," Tech. Rep. 38, White Sands Missile Range, White Sands, NM, 1972.

[10] Schmidt, S. F., "Application of State-Space Methods to Navigation Problems," *Advances in Control Systems*, Vol. 3, 1966, pp. 293–340, doi: 10.1016/B978-1-4831-6716-9.50011-4.

[11] Zanetti, R. and D'Souza, C., "Recursive Implementations of the Consider Filter," *Journal of the Astronautical Sciences*, Vol. 60, No. 3–4, July–December 2013, pp. 672–685, doi: 10.1007/s40295-015-0068-7.

[12] J.L., and Markley, F.L., "Three-Axis Attitude Estimation Using Rate-Integrating Gyroscopes," *Journal of Guidance, Control, and Dynamics*, Vol. 39, No. 7, 2016, pp. 1513–1526, doi: 10.2514/1.G000336.

[13] Ignagni, M. B., "Efficient Class of Optimized Coning Compensation Algorithms," *Journal of Guidance, Control, and Dynamics*, Vol. 19, No. 2, March–April 1996, pp. 424–429, doi:10.2514/3.21635.